Modification of continental lithosphere by tectonic processes: A tomographic image of central North America

A. W. Frederiksen,[1] T. Bollmann,[2] F. Darbyshire,[3] and S. van der Lee[2]

Received 10 September 2012; revised 18 December 2012; accepted 19 December 2012; published 22 March 2013.

[1] The assembly of Laurentia by Precambrian accretion is also believed to have formed the underlying lithosphere. Accretionary signatures are detectable by seismic observations but subject to modification by later processes, e.g., orogeny, rifting, and plumes. We examine the Archean Superior Province (SP) and environs using a set of teleseismic *P* wave arrivals from Canadian and American instruments. The resulting tomographic model has high resolution beneath the Dakotas and Minnesota, provides a first look at the lithosphere beneath Manitoba, and sharpens previously documented features in Ontario. From the model and previous anisotropy observations, we detect (i) a large high-velocity feature beneath the western SP, associated with elevated lithospheric anisotropy. The high-velocity feature does not match crustal boundaries; notably, its western edge lies approximately 200 km east of the contact with the Proterozoic Trans-Hudson Orogen (THO). (ii) A low-velocity channel-shaped feature strikes northwest through Minnesota and the Dakotas, associated with weakening anisotropy. (iii) High velocities southwest of (ii), beneath the Minnesota River Valley terrane (MRVT), associated with low anisotropy. We interpret (i) to be accretionary, and contemporaneous with Superior assembly; similar velocity but weaker anisotropy of the MRVT is consistent with vertical-tectonic mechanisms. The inboard location of the THO contact may indicate modification of the Superior root. The low-velocity channel has no obvious crustal expression but connects to an offset in the Proterozoic Mid-Continent Rift (MCR) and may be rift related. The MCR is not well imaged but will be examined via the temporary Superior Province Rifting EarthScope Experiment, in progress.

Citation: Frederiksen, A. W., T. Bollmann, F. Darbyshire, and S. van der Lee (2013), Modification of continental lithosphere by tectonic processes: A tomographic image of central North America, *J. Geophys. Res. Solid Earth*, *118*, 1051–1066, doi:10.1002/jgrb.50060.

1. Introduction

[2] Cratonic regions of the Earth's crust are typically associated with high seismic velocitities in the upper 200–300 km, believed to represent the lithospheric portion of the cratonic root or keel. These roots are thought to be cold, depleted remnants of the cratonization process [*Jordan*, 1978; *Pearson and Wittig*, 2008] and so are presumably coeval with the overlying crust. In the case of Archean cratons, the lithospheric root would then have been stable for 2.5 Ga or more.

[3] Cratonic roots are not, however, immune to the influence of external tectonic and convective events. Orogenic events at the edges of stable cratons may have effects extending a significant distance into the cratonic interior [e.g., *Zhang et al*., 2003; *Zhu and Zheng*, 2009]. Upwelling mantle plumes may heat, alter, underplate, or erode the lithosphere [*Rondenay et al*., 2000; *Foley*, 2008], while continental rifting may thin or divide it. All of these processes have the potential to leave evidence within the lithosphere itself, which may be detected in situ by geophysical means. In this paper, we examine the southwestern edge of the Superior craton in central North America and demonstrate that high-resolution tomography can help determine the history of the lithosphere and its relation to crustal tectonic events.

2. Background

[4] Central North America (Laurentia) is Precambrian in age. It is an assemblage of Archean microcontinents amalgamated via Proterozoic orogens, the largest of these Archean blocks being the Superior Province (Figure 1, inset) [*Hoffman*, 1989]. The Superior is bounded to the west and north by the Trans-Hudson Orogen, which stabilized ca. 1.8 Ga. At the Superior's southern edge, the Penokean orogen, similar in age to the Trans-Hudson [*Schulz and Cannon*, 2007], was crosscut by the ca. 1.1 Ga Mid-Continent Rift [*Van Schmus and Hinze*, 1985;

[1]Department of Geological Sciences, University of Manitoba, Winnipeg, Manitoba, Canada.
[2]Department of Earth and Planetary Sciences, Northwestern University, Evanston, Illinois, USA.
[3]Centre de recherche GEOTOP, Université du Québec à Montréal, Montréal, Québec, Canada.

Corresponding author: A.W. Frederiksen, Department of Geological Sciences, University of Manitoba, Winnipeg, Manitoba, Canada. (frederik@cc.umanitoba.ca)

2169-9313/13/10.1002/jgrb.50060

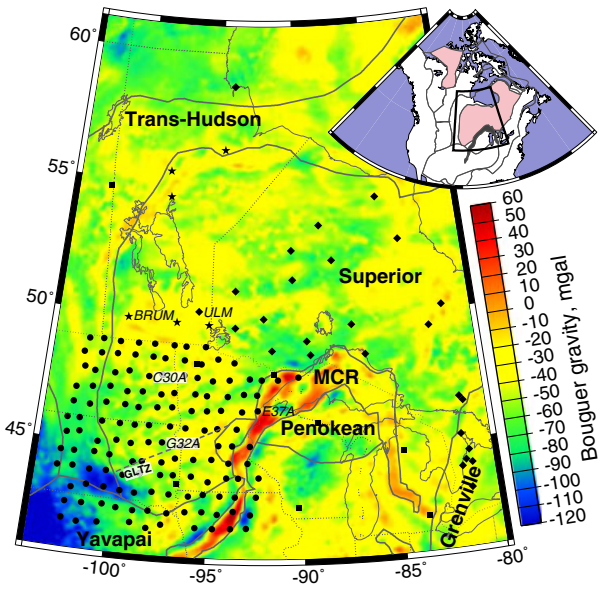

Figure 1. Inset: study area (box) in relation to major tectonic divisions of North America (after *Hoffman* [1988]; stable Archean cratons in pink). Main map: instruments contributing to this study's data set, overlain on a Bouguer gravity map. Diamonds are stations from the Canadian National Seismograph Network, POLARIS Ontario, or FedNor networks; squares are permanent IRIS-operated stations (Global Seismographic Network or United States National Seismic Network); circles are USArray Transportable Array stations; stars are stations operated by the University of Manitoba. Labeled stations are mentioned in the text. Gravity data are from the Decade of North American Geology gravity grid [*Tanner et al*., 1988]. Selected tectonic boundaries on the main map were digitized from *Whitmeyer and Karlstrom* [2007]. MCR: Mid-Continent Rift; GLTZ indicates the approximate location of the Great Lakes Tectonic Zone.

Ojakangas et al., 2001]. The degree to which these tectonic events affected the lithosphere remains somewhat unclear.

[5] The western Superior Province is subdivided into east-west trending sub-provinces, representing terranes or terrane assemblages that accreted progressively from north to south ca. 3.0–2.7 Ga [*Card and Poulsen*, 1998; *Percival et al*., 2006]. These sub-provinces consist primarily of granite-greenstone, metasedimentary, and plutonic belts, with the notable exception of the high-grade gneisses of the Minnesota River Valley Terrane, in the southwest corner of the Superior. The accretion of these sub-provinces affected the lithosphere, as evidenced by the presence of Moho-crossing reflectors at suture zones [*Calvert et al*., 1995; *Calvert and Ludden*, 1999; *White et al*., 2003] and slab-like sub-crustal bodies [*Musacchio et al*., 2004]. Following accretion, the Superior Province was affected by orogenic activity at its edges, uplift and crustal shortening along the Kapuskasing structural zone [*Percival and West*, 1994], and multiple Proterozoic dyke swarms [*Osmani*, 1991].

[6] The oldest and westernmost of the orogens bordering the Superior is the Trans-Hudson Orogen, a complex Himalayan-scale orogeny resulting from the closure of the Manikewan Ocean and collision of the Superior craton with the Hearne and Wyoming cratons ca. 1.85–1.78 Ga [*Ansdell*, 2005; *Whitmeyer and Karlstrom*, 2007], trapping the smaller Sask Craton and Medicine Hat Block. The complex nature of the collision implies a high degree of lateral variation along the strike of the Trans-Hudson, but due to its limited surface exposure (much of the Trans-Hudson lies underneath sedimentary cover in the Western Canada Sedimentary Basin and Hudson Bay), the structure of the Trans-Hudson crust and lithosphere is only well understood in limited areas. The Lithoprobe Trans-Hudson Orogen transect imaged the orogen in Manitoba and Saskatchewan using controlled-source [*Németh et al*., 2005] and teleseismic [*Bank et al*., 1998] techniques, finding indications of crust-mantle detachment and lateral variations within the Trans-Hudson lithosphere. More recent work in Hudson Bay shows thick lithosphere but no systematic change across the Superior/Trans-Hudson boundary [*Darbyshire and Eaton*, 2010].

[7] To the southeast, the Superior is truncated by the overlapping effects of the Penokean Orogen and the Mid-Continent Rift. The Penokean Orogen records collisions and continental growth at the southern margin of Laurentia ca. 1.88–1.83 Ga [*Schulz and Cannon*, 2007] but has been extensively overprinted by later tectonic activity. The largest source of overprinting was the ca. 1.1 Ga Mid-Continent Rift (MCR) system, also known as the Keweenawan Rift [*Van Schmus and Hinze*, 1985]. The MCR formed a ca. 2000 km long segmented rift system featuring extensive magmatism, broad subsidence, and basin formation [*Ojakangas et al*., 2001]. The rifting process never reached the point of developing an ocean basin, and the rift eventually closed, perhaps due to Grenvillian orogenesis [*Cannon*, 1994]. The MCR is responsible for a major gravity anomaly (Figure 1), presumably the result of magmatism, the crustal structure of which was examined by the Great Lakes-focused GLIMPCE project [see, e.g., *Mariano and Hinze*, 1994; *Sexton and Henson*, 1994]. There is geochemical evidence [e.g., *White*, 1997; *Nicholson et al*., 1997] suggesting a significant mantle plume contribution to MCR basalts, which would imply a modified or thinned lithosphere beneath the rift, but the MCR lithosphere has not been imaged in detail.

[8] The work presented here follows up on a study by *Frederiksen et al*. [2007] which used seismic tomography and shear-wave splitting to image the mantle across the Superior Province. The previous study detected high-velocity, strongly anisotropic lithosphere beneath the western Superior, bounded at ≈ 88°W by lower-velocity lithosphere to the east, and interpreted to be influenced by the Great Meteor hot spot track. A small low-velocity lithospheric feature underlies the Nipigon Embayment, a magmatic region north of Lake Superior which is contemporaneous with the MCR and is believed to share a common origin with it, though the lack of extensional features in the embayment indicates that it is not a failed rift arm in the usual sense [*Hart and MacDonald*, 2007]. Magnetotelluric studies also indicate that the mantle beneath the Nipigon Embayment is anomalous [*Ferguson et al*., 2005]. If the Nipigon Embayment shares a common origin with the MCR, the existence of a Nipigon lithospheric anomaly suggests that anomalous upper mantle may also underlie the MCR.

[9] The *Frederiksen et al*. [2007] study was largely restricted to data from Ontario and so was not able to image the southern and western edges of the Superior Province. In particular, it left unaddressed the issue of whether the high

velocities and strong anisotropy in the western Superior were a feature localized to the Superior Province itself or represented conditions typical of the western Canadian Shield. The advent of EarthScope data from the United States [*Williams et al*., 2010], along with the installation of additional instruments in Manitoba, allows for a westward and southward extension of the earlier project, crossing the Superior Province's boundaries with the Trans-Hudson and Penokean orogens as well as the Mid-Continent Rift. The goal of this study is therefore to examine the lithospheric expression of these tectonic boundaries through tomographic means. We have defined a study area (Figure 1), centered on the western Superior, which exploits the new data set to best advantage, and will allow the future incorporation of data from the SPREE project [*Stein et al*., 2011].

3. Data Set

3.1. Instrumentation

[10] The Canadian portion of the subject area has been instrumented by the digital Canadian National Seismograph Network (CNSN) since the 1990s [*North and Basham*, 1993]. This network was supplemented by instruments of the POLARIS [*Eaton et al*., 2004] and FedNor [*Darbyshire et al*., 2007] temporary deployments, several of which have since been established as permanent CNSN stations. Data from these Canadian stations were the basis for a previous tomographic study in the area [*Frederiksen et al*., 2007]. The present study uses all available CNSN, POLARIS, and FedNor data for the study area for the period from 1 January 2006 to 15 April 2011 (Figure 1, diamonds).

[11] As mentioned above, the 2007 study imaged structures within the Superior Province but did not have resolution across its western and southern boundaries. In order to examine the Superior's southern boundary with the Mid-Continent Rift, data from the United States were used. The number of American stations available in the study area has greatly expanded due to the EarthScope project [*Williams et al*., 2010] and the arrival of the Transportable Array in the mid-continent. Figure 1 shows the EarthScope stations available over the 1 January 2006–15 April 2011 study period (circles) along with a small number of permanent stations which were also analyzed (squares).

[12] The western boundary between the Superior Province and the Trans-Hudson Orogen lies in Manitoba, which is very poorly instrumented by permanent stations (two CNSN stations, FCC and ULM, are in Manitoba, and station FFC of the Global Seismographic Network is located near the Manitoba-Saskatchewan border). To address this issue, University of Manitoba researchers deployed seven Guralp CMG-3TD broadband instruments in Manitoba in 2007, six of which successfully returned data (Figure 1, stars). The northern instruments experienced reliability problems and recorded for relatively short periods (averaging around six months), while the southern instruments (including BRUM, which is labeled in the Figure) were more reliable and are still in operation as of this writing.

[13] The date range of data used in this study was not chosen arbitrarily. The 1 January 2006 start date was selected so as to not overlap with a previous study [*Frederiksen et al*., 2007] which ended in 2005 and to cover the period of recording of all University of Manitoba instruments. The end date (15 April 2011) coincides with the beginning of a temporary experiment in the study area: project SPREE (Superior Province Rifting EarthScope Experiment) [*Stein et al*., 2011; *Van der Lee et al*., 2011]. SPREE is a deployment of EarthScope Flexible Array instrumentation in the United States and Canada, targeting the Mid-Continent Rift. It consists of 83 stations in total: 16 stations in Canada, widely spaced (approximately 100 km apart) around Lake Superior to complement the EarthScope Transportable Array instruments in the United States, and 67 closely spaced (approximately 10 km) stations in the United States, in lines following and crossing the rift axis in Minnesota and Wisconsin. We expect SPREE data to greatly improve resolution of the rift and environs in tomographic models. However, the SPREE instruments are non-telemetered and will only return data at 6 month servicing intervals. The full SPREE data set will not be available until late 2013; therefore, SPREE data will be considered at a later date, and this study will examine the state of knowledge prior to the SPREE project.

3.2. Traveltimes

[14] Relative traveltimes were measured using *P* wave first arrivals (teleseismic *P*, and occasionally *Pdiff*) at all stations recording a given event. Instrument responses were removed from the traces, which were then filtered in a narrow band (typically 0.6–6 Hz, though the filters were modified in some cases to accommodate varying frequency contents and noise environments). The traveltimes were measured using the multichannel cross-correlation method of *VanDecar and Crosson* [1991]. This type of traveltime measurement yields relative traveltimes with a zero event mean; that is, the observed traveltime for event i and station j is

$$t_{ij} = T_{ij} - \bar{T}_i \tag{1}$$

T_{ij} being the true traveltime and $\bar{T}_i$ being the (unknown) average of all traveltimes for the ith event. For plotting purposes, the measured relative traveltimes were compared to predictions from model IASP91 [*Kennett and Engdahl*, 1991] by subtracting the IASP91 predictions from the measured times:

$$\delta t_{ij} = t_{ij} - T_{ij}^{IASP91} + \bar{T}_i^{IASP91} \tag{2}$$

[15] By adding back the average IASP91 traveltime $\bar{T}_i^{IASP91}$, we generate residuals δt_{ij} that have zero event mean and may be compared between events. Figure 2a shows traveltimes (relative to IASP91) for a magnitude 7.1 earthquake from Japan. Even from a single event, the station density is sufficient to show a significant amount of structure, notably early arrivals (indicating high average velocity) in western Ontario and late arrivals in the southeastern and southwestern corners of the study area.

[16] A total of 942 earthquakes (of magnitude 5.5 or greater, 30°–100° from the centre of the study area) were picked at a total of 180 stations, giving a total of 49,844 traveltime picks. Figure 2b shows the number of picks recorded for each station. The number of picks for a given station is mostly determined by the installation time—note that the long-operating Canadian stations have the most recorded picks (the largest number is 880 picks at CNSN station ULM, Lac du Bonnet, Manitoba, which operated

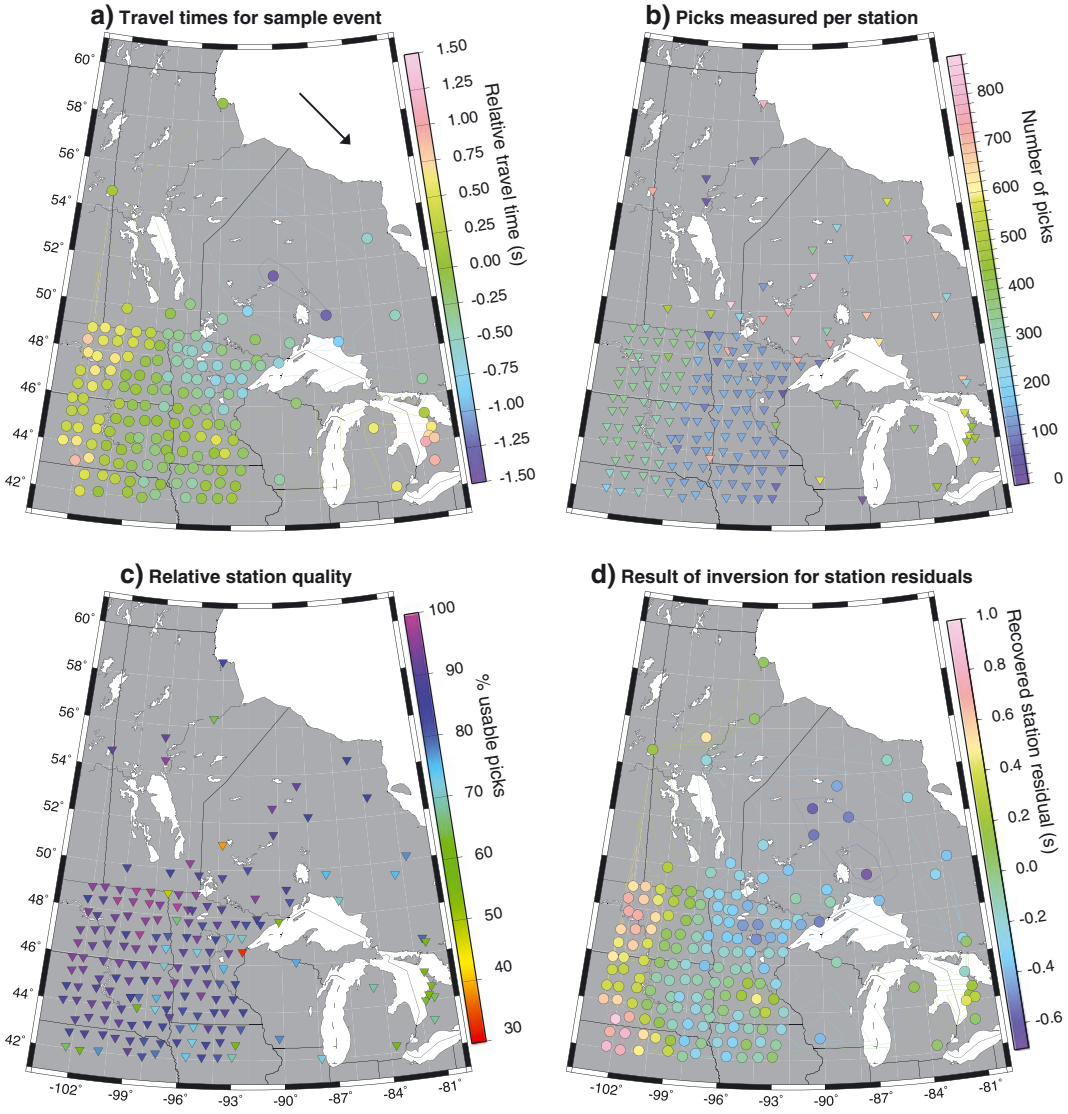

Figure 2. Some characteristics of the traveltime data set. (a) Map of relative traveltime residuals (with respect to IASP91 predictions) for a single event (Japan, 7 April 2011, 14:32:43); the arrow shows the direction of wave propagation. (b) Number of traveltimes measured at each station. (c) Relative quality of each station, measured as the percentage of recorded events which gave usable traveltime picks. (d) Result of a simple inversion for station residuals (see text for inversion procedure).

continuously throughout the study period and is located in a quiet shield environment). The directional sampling of the data set is quite broad, particularly at the longer-operating stations (Figure 3), though there is a significant gap in the western to southwestern back-azimuth range. Noise levels may be compared by dividing the number of usable picks by the number of available traces at a given station, giving a percentage (Figure 2c). Most stations were high quality (>70% of available data picked), though there is clearly a higher noise level in southern Ontario (southeast corner of study area), perhaps due to cultural noise or microseismicity as the area is both densely populated and seismically active. Some individual stations had high noise levels (the worst being EarthScope station E37A with 33% pickability), presumably due to localized site problems.

[17] Prior to performing a tomographic inversion, we examined the geographic pattern of traveltimes by carrying out a simple inversion for station corrections. A traveltime residual t_{ij} (relative to the prediction from standard model IASP91) for event i and station j may be taken to be a combination of station and event terms:

$$t_{ij} = e_i + s_j \tag{3}$$

wherein the event term corrects for both structure on the source side and the relative nature of the traveltime measurement (the unknown $\bar{T}_i$ in equation (1)). Posing this equation as a linear inverse problem for both e_i and s_j, with damping applied to the station corrections, gives a zero-mean pattern of station terms as consistent as possible with all measurements. The result of this inversion is shown in Figure 2d. The pattern of station terms should in principle be controlled entirely by receiver-side structure (including the lithosphere, crust, and site response) but has no depth resolution. We can

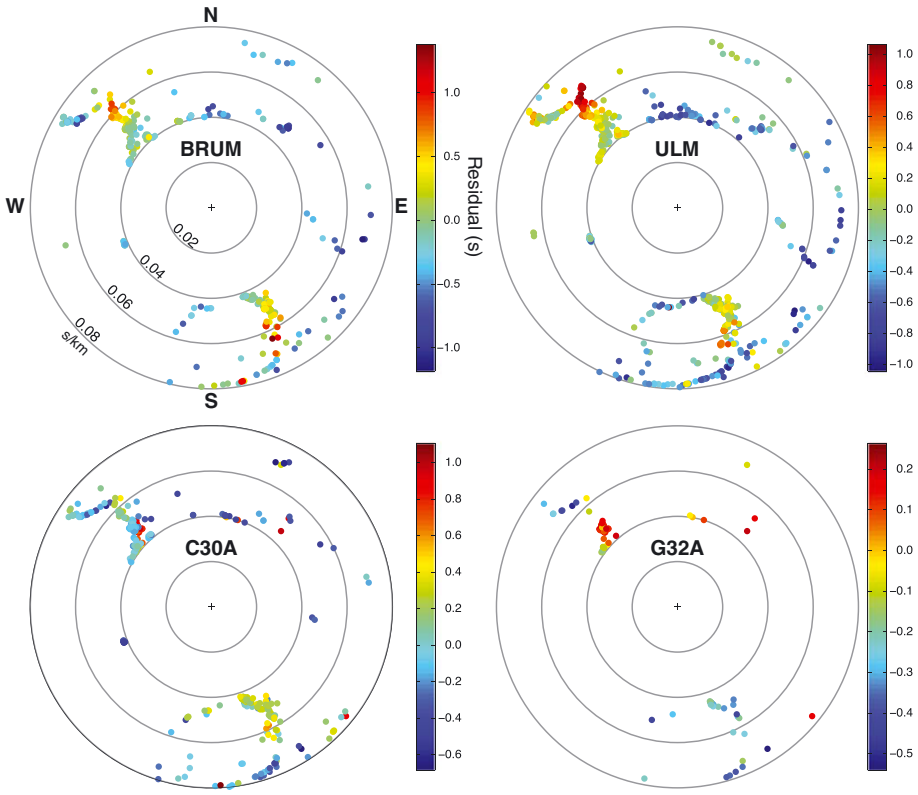

Figure 3. Residuals at individual stations after removal of station/event terms, plotted by ray direction at the station. Azimuth shown is the back azimuth from the station to the source; the radius is the slowness predicted by the IASP91 model. Shading of points indicates traveltime residuals, with positive values representing late arrivals (i.e., lower-than-average velocities). See Figure 1 for the locations of these stations.

see that the most negative station terms (representing early arrivals and presumably high velocities) occur in western Ontario (exposed shield), while positive (slow) terms are seen in sedimentary basins: southern Ontario and especially the western Dakotas.

[18] Once station and event terms have been determined, any remaining traveltime residuals will be due to either measurement error or 3-D structure in the receiver-side mantle; if 3-D structure is present, the residual pattern should be spatially coherent. To test this, we examined the traveltime residuals of individual events after subtraction of event and station terms. Figure 3 shows directional plots of these residuals. The residuals appear directionally coherent, implying that the traveltime variations detected are due to 3-D structure rather than picking error. The directional patterns are also indicative of the types of structures that we should expect to see in a tomographic model. For example, station ULM has higher velocities to the north and northeast than to the northwest; BRUM has isolated low-velocity features to the northwest and southeast; C30A and G32A have low velocities to the southeast and northwest, respectively, implying that a low-velocity feature lies between the two.

4. Tomographic Model

4.1. Basis

[19] As Figure 3 shows, our teleseismic data set is not adequately represented as a sum of station and event corrections, as the residuals are significant and directionally coherent. Properly speaking, the traveltime equation should contain a path component [*VanDecar*, 1991]:

$$t_{ij} = e_i + s_j + p_{ij} \tag{4}$$

where p_{ij} is a term representing the effect of 3-D structure. At teleseismic distances, ray paths in the crust will be close to vertical (particularly in low-velocity sedimentary layers) and so would not vary much between events, being mostly accounted for by the station correction s_j. In addition, since the source-receiver distance is much greater than the array aperture, the rays near the source will be very similar (Figure 4), and so source-side structure will be taken up by the event correction e_i.

[20] The middle sections of the ray paths in Figure 4 are significantly different and therefore may be contributing to the observed directional variations in traveltime. However, global tomographic models generally show weak velocity variations in the mid-mantle compared to the upper mantle [see, e.g., *Li et al.*, 2008]. We can therefore reasonably expect upper mantle structure to account for the bulk of the directional variations. For this project, the aperture of the array is quite large, and therefore, we can expect some crossing rays in the mid-mantle, though the densest ray concentrations will be in the upper mantle. We therefore extend the model volume down to 1500 km depth, below most ray crossings, in order to prevent any mid-mantle structure from being incorrectly mapped into the upper mantle.

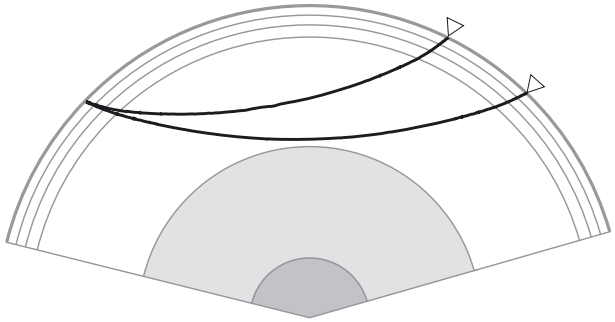

Figure 4. Ray paths from the event shown in Figure 2a to the closest and most distant station.

We will not, however, interpret any features below the transition zone and will concentrate our interpretation on lithospheric depths. To further prevent structures outside the model volume from contaminating our model, we extend the model grid approximately 300 km beyond the footprint of the instrument array, though we will need to bear in mind that structures outside of the array footprint are not safe to interpret.

4.2. Inversion Parameters

[21] For the tomographic inversion, we used the well-established method of *VanDecar* [1991]. The model is parameterized in terms of deviations from IASP91 P velocity on a set of tensioned splines, smoothly interpolating between the nodes of a spherical grid (Figure 5). We used a horizontal node spacing of 1/4° (≈28 km) in latitude and 1/3° (≈29 km at 39°N) in longitude, with wider spacing used at the edge of the model (where we do not expect to resolve structure). A vertical node spacing of 25 km was used for the uppermost 200 km of the model, increased to 33 km from 200 to 700 km, to 50 km from 700 to 800 km, and to 100 km from 800 km down to the model base at 1500 km depth. The model thus totaled 221,859 grid nodes, though the total number of unknowns was greater

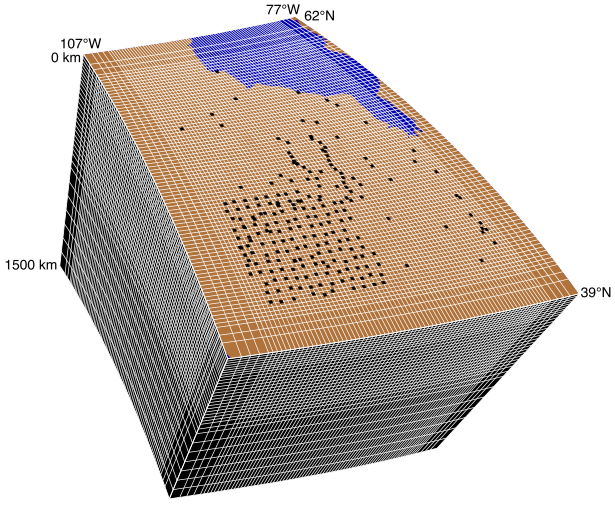

Figure 5. Model grid used in the tomographic inversion. Grid nodes are located at the intersections of the white lines; between the nodes, the model is interpolated using splines under tension [*VanDecar*, 1991]. Black squares are station locations.

than this due to the incorporation of station and event terms as well as perturbations to the event location, all of which were allowed to vary.

[22] The method of *VanDecar* [1991] is purely ray theoretical. Given the growing recognition of the importance of finite-frequency effects in tomography [see, e.g., *Liu and Gu*, 2012 for a recent review], our use of ray theory merits some justification. Finite-frequency effects result from kernels whose width increases with wavelength; though the classical Fresnel zone does not exactly correspond to an accurate finite-frequency kernel, it approximates the volume affected by the ray. Assuming a frequency of 3 Hz (at the center of the passband used in this study), and a ray length of 9700 km (the approximate length of the ray corresponding to a *P* wave at 98° source-receiver distance), the first Fresnel zone will be about 42 km wide at 300 km depth. This is significantly smaller than the ≈70 km spacing of Transportable Array stations and considerably smaller than the effective resolution of this study (approximately 100 km; see below); we conclude that any finite-frequency effects in this data set will be at a scale smaller than our ability to resolve and that ray-theoretical tomography will be sufficiently accurate.

[23] For inversion purposes, a few traveltimes were removed from the data set. The removed times represented situations that the tomography software could not handle, such as the presence of both P and Pdiff picks for the same event (the phase with the most picks was retained). The inversion was therefore performed using 49,298 new traveltime picks. We augmented our new data set with data from the previous study of *Frederiksen et al*. [2007] falling within the study area, including FedNor and CNSN data from 2003 to 2005 (2788 picks out of the original 4048), picks from the 1997 Teleseismic Western Superior Transect (TWST) temporary deployment [*Sol et al*., 2002] (1412 picks), and picks from the 1989 APT89 experiment [*Silver et al*., 1993] (649 picks). The APT89 data were re-picked for this study, as the study area for this project extends further southwest than that considered in the *Frederiksen et al*. [2007] study and therefore includes more of the APT89 stations.

[24] Figure 6a shows a plan section through the model obtained by inverting the new data only, while Figure 6b shows the equivalent section through a model obtained using the combined data set (totaling 54,147 picks). Comparing the two, it is clear that the new data are the source of most of the structural information in the model but that the older data make a positive contribution to the model's resolution (particularly due to the dense linear coverage of the TWST and APT89 data sets). The combined data set was therefore used in all further work.

[25] The combined data set consists of 220 stations and 1403 earthquakes. Each station adds an additional free parameter (the station time correction) to the inversion, while each earthquake adds four parameters (the event time correction and the event mislocation in three dimensions). Added to the number of grid nodes, the inverse problem thus has 227,691 unknowns and is clearly strongly underdetermined. The images obtained by inversion will therefore be strongly dependent on the nature and strength of the regularization used. We applied a smoothing regularization (minimizing model curvature) to the model, as is common in mantle tomography, in order to favor long-wavelength structure in the final

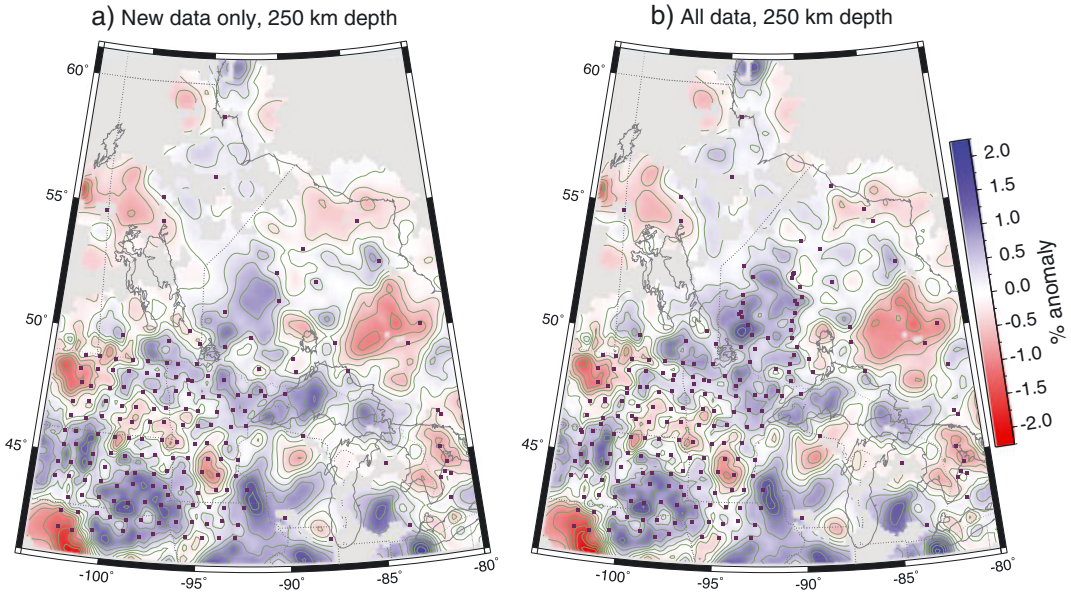

Figure 6. Comparison of inversion results using (a) new data from this study only and (b) new data plus picks from previous studies. Purple squares represent locations of stations used in the inversion. See text for details of the previous studies.

model; small amounts of flattening (slope minimization) and damping (minimization of deviation from IASP91) were also included, in order to stabilize the numerical problem. Event location perturbations and station time corrections were also damped, while event time corrections were left undamped (to compensate for the relative nature of the time picks).

[26] The level of smoothing applied to the entire model was chosen using the so-called "L-curve" method, in which model roughness is plotted against data misfit for a number of different smoothing levels [*Parker*, 1994]. The resulting curve typically exhibits a change in slope at the point where decreasing the regularization level leads to noise, rather than signal, being fit; the appropriate regularization level to use is generally taken to be at or near the slope change. The smoothing level chosen implies an RMS misfit of ≈56 ms, which is a plausible value (corresponding to about two samples at a 40 Hz station). The damping level for station time corrections was determined separately by comparing the recovered time corrections to corrections predicted from the global crustal model Crust2.0 [*Bassin et al.*, 2000]; though the Crust2.0 predictions are not likely to be accurate due to limited crustal model resolution in the study area, their range of variation should be indicative of the correct range of crustal timing corrections.

4.3. Resolution

[27] In principle, the resolution of a linear inverse problem is completely defined by the resolution matrix, which maps true structures to recovered models [*Parker*, 1994]. Since the resolution matrix maps between points in model space, it will have a number of elements equal to the square of the number of unknowns, which in this case would be approximately 5.2×10^{10} elements—clearly, determining the full resolution matrix is impractical for problems of this size. Instead, we resort to more qualitative approaches for resolution measurement which are common practice in seismic tomography.

[28] The resolution problem in tomography amounts to two separate questions: to what degree and in what manner are features likely to be smeared, and what minimum size of feature can be resolved at different points in the model volume? The latter question can be approached by forward modeling through models containing localized features in the volume of interest and inverting the resulting synthetic. An efficient approach is to use a three-dimensional "checkerboard" of anomalies with alternating polarities, thus measuring the resolution of the whole model at a particular spatial wavelength. We performed checkerboard resolution tests using alternating Gaussian anomalies reaching ±2% of background velocity at two different 3-D spacings: 200 and 100 km. Random perturbations were added to the data to match the 56 ms RMS noise level obtained from the real data via the L-curve.

[29] Figure 7a shows a horizontal slice through the fine (100 km spacing) checkerboard input model. The checkerboard pattern is three dimensional, with anomalies centered at depths of 50, 150, 250,. . ., so slices at any of those depths would look the same (except for an alternation of anomaly polarities). At 50 km (not shown), anomaly recovery is poor, probably due to the tradeoff between shallow structure and station terms. Figures 7b–7e shows outputs at depths from150 to 450 km. It is clear from these plots that resolution at the 100 km feature scale is achieved at lithospheric depths within the region of dense station coverage (the Transportable Array footprint, the two station lines in western Ontario, and a small area in southern Ontario) and not elsewhere. Some smearing with a northeast-southwest grain is visible (particularly at shallower depths) and is presumably reflective of the dominant directions of back-azimuthal coverage. A coarser checkerboard with 200 km anomaly spacing (Figure 7f) is better recovered, with reasonable recovery of lithospheric anomalies throughout most of the study area, the exceptions being the northwest corner (where station coverage is limited) and the area south of the Great Lakes.

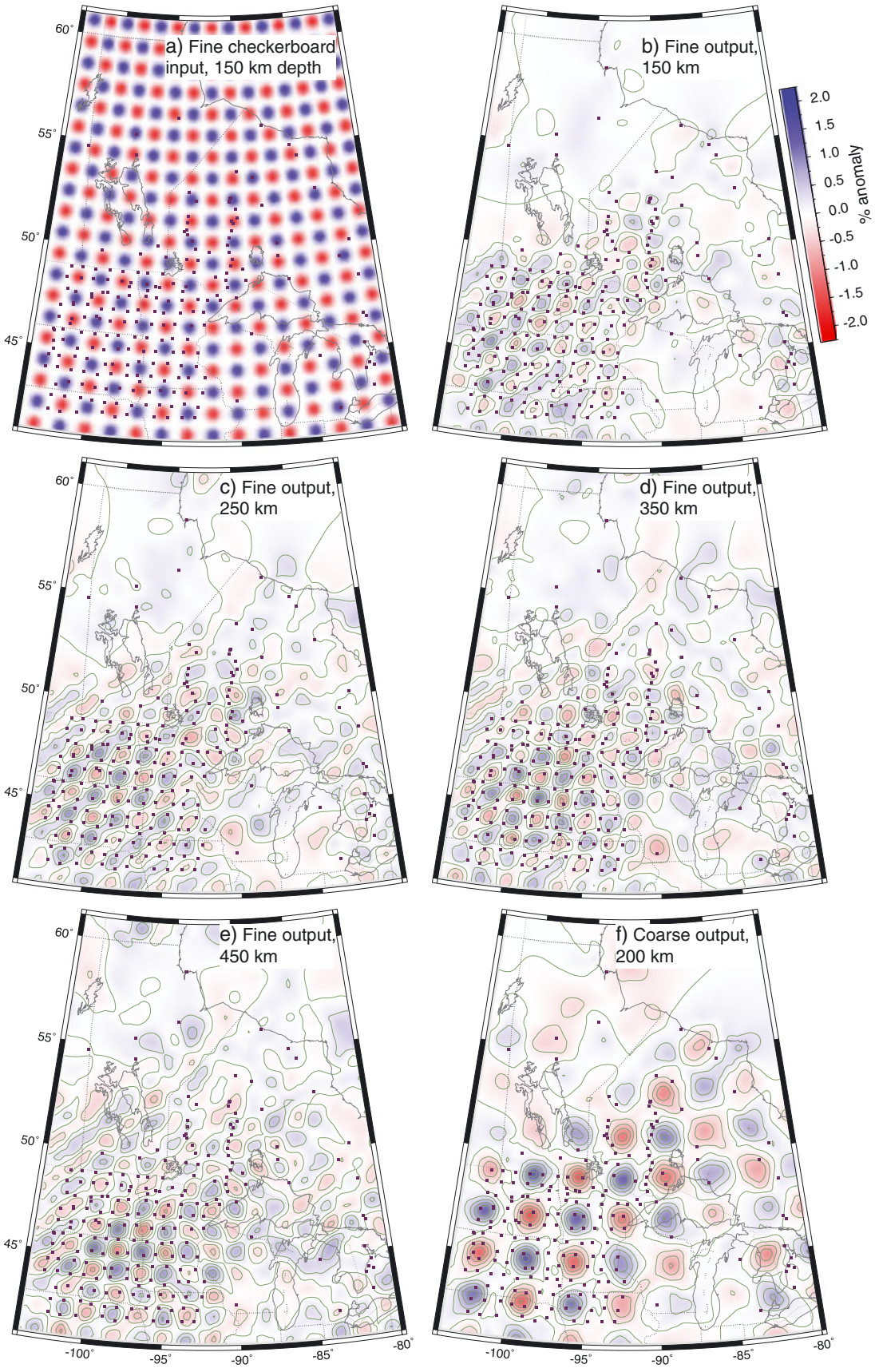

Figure 7. Selected results from two checkerboard tests. (a) Plan section through fine input model with 100 km anomaly spacing; (b–e) plan sections through fine output model; (f) plan section through coarse output model (200 km anomaly spacing).

[30] As noted above, these checkerboard tests determine the ability to resolve small features but do not address the degree of smearing experienced by larger features. Such smearing is best detected by synthetic tests in which simplified structures resembling observed features are modeled. The results of this type of test will be shown once the relevant features have been identified.

4.4. Major Features of the Model

[31] A series of plan sections through the final model are shown in Figure 8. Figure 8a includes a plot of the station terms; the main feature of the station terms is that the largest values were assigned to stations from previous short-term deployments (TWST and APT89). This phenomenon is presumably a consequence of the TWST and APT89 deployment periods not overlapping with the other stations, and so their traveltimes being measured with respect to a different effective baseline; in any event, it is clear from Figure 6 that the large station terms for these stations do not indicate a problem affecting the 3-D model. Station terms for the longer-operating instruments vary slowly across the study area and have a pattern consistent with the shield-platform transition from northeast to southwest: early arrivals (more negative station terms) in the shield and increasingly late arrivals into the sedimentary basins.

[32] The largest lithospheric anomaly in the model is a high-velocity region labeled as feature A in Figure 8b. It is a roughly triangular high-velocity block that appears to be at least 300 km thick (Figure 9), with a well-resolved eastern boundary running approximately N-S at about 88°W. Its southern boundary runs WNW-ESE, centered approximately on 47°N and is also well resolved, while its northwest boundary is more poorly resolved (lying in a gap in station coverage). To the east of feature of A are two low-velocity regions labeled B and C. B is a small low-velocity, near-surface (it disappears just below 200 km in cross-section A-A′, Figure 9) feature, while C is a larger low-velocity zone that extends below 300 km.

[33] Feature A is truncated to the southwest by a linear low-velocity channel labeled D. Feature D is about 150–200 km across, begins at approximately 45°N, 94°W and extends northwest to the western limit of the model's resolution. It extends to an apparent depth of 300–400 km (Figure 9, section D-D′). Southwest of D lies another high-velocity

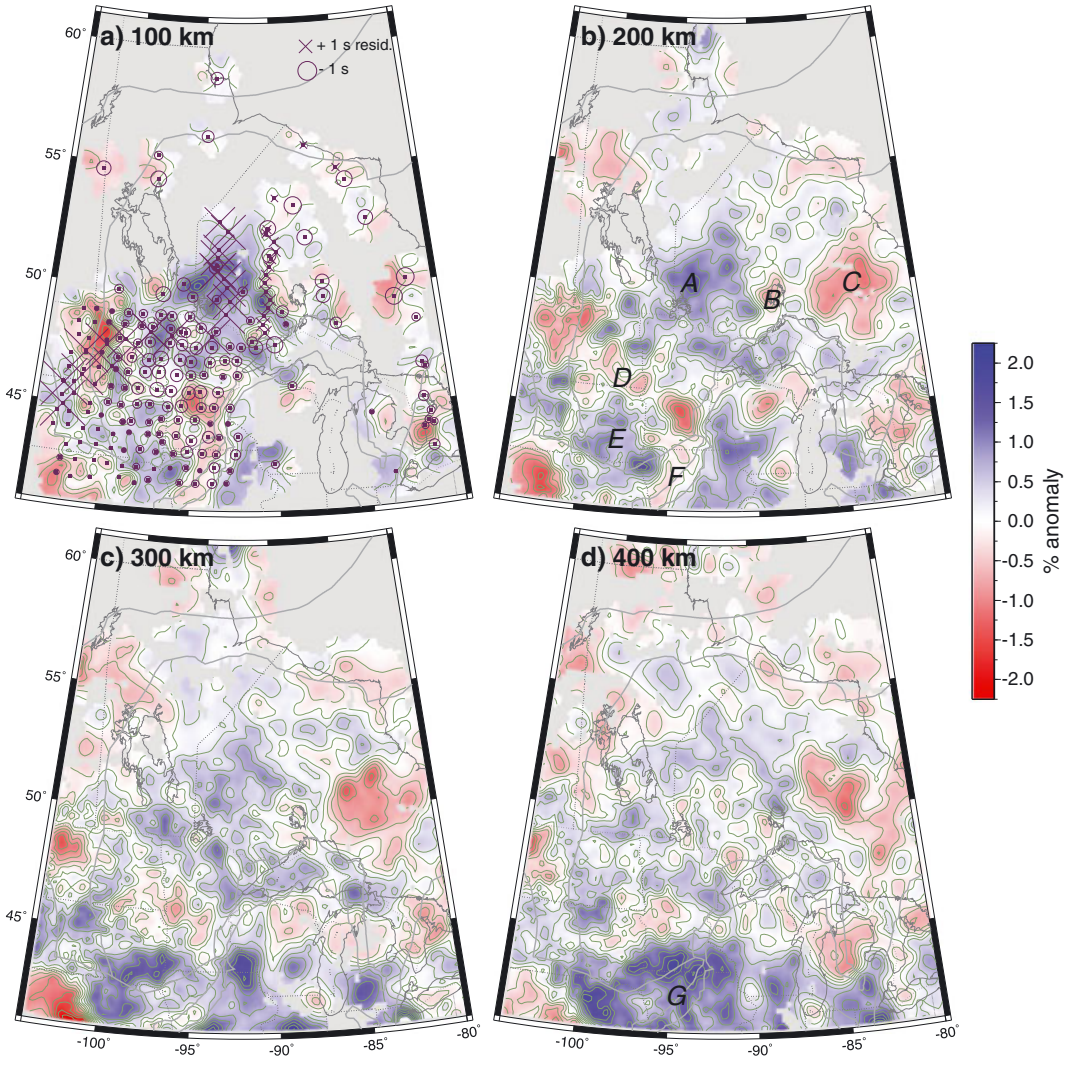

Figure 8. Plan sections through the final model, at 100 km intervals. Figure 8a includes the station terms; features discussed in the text are labeled in Figures 8b and 8d.

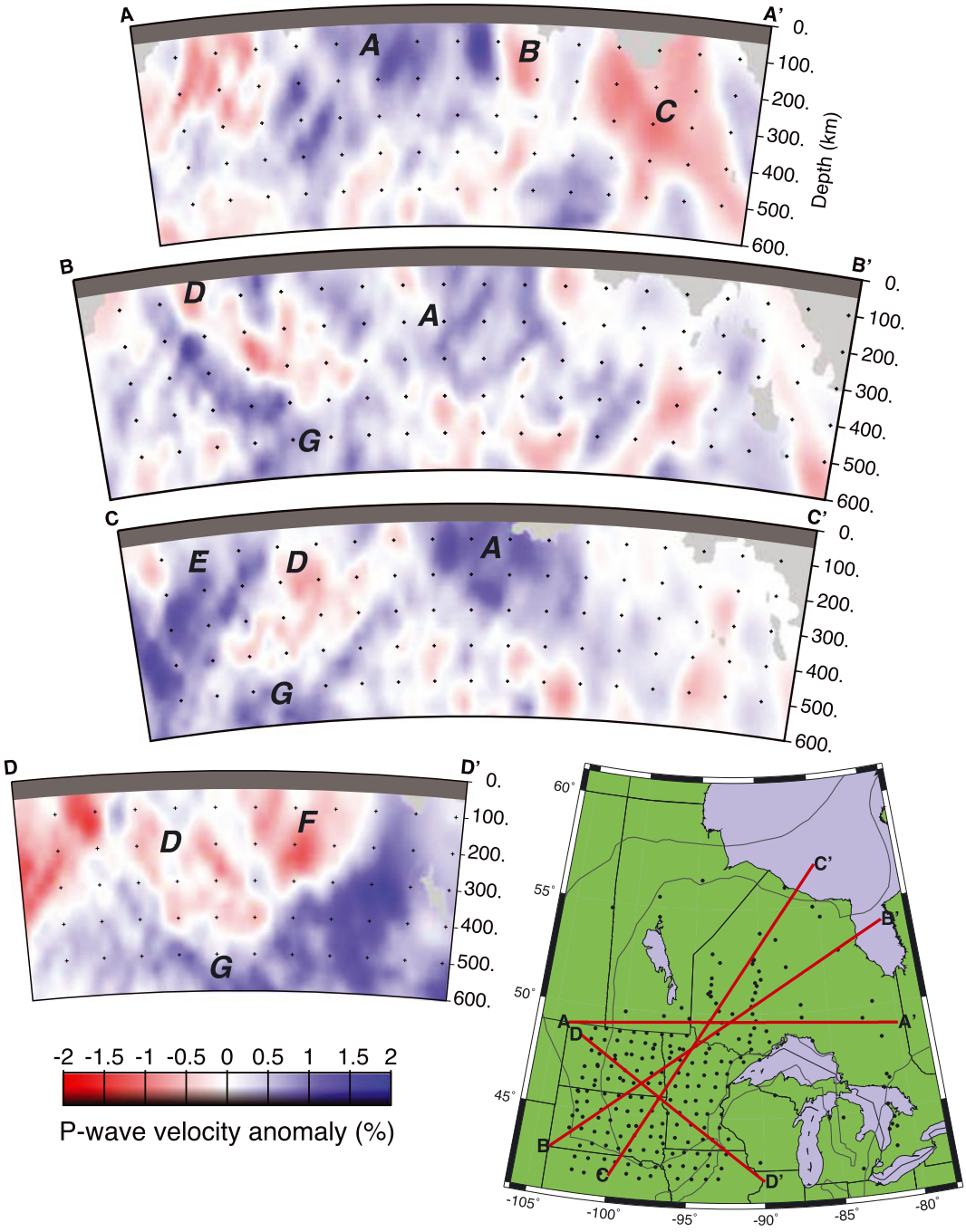

Figure 9. Cross-sections sections through the upper 600 km of the final model. The map at bottom shows the cross-section locations. Labeled features are the same as in Figure 8.

region (E), comparable to A in thickness (section A-A′), whose southern and western limits are not imaged. East of E, a second low-velocity channel (F), comparable to D in appearance extends south from the southeastern edge of D to the model's southern boundary.

[34] The model contains significant resolution at depths below the lithosphere. One significant feature (G) shows up at 400 km depth in the southern section of the model (Figure 8d). G is an extensive high-velocity anomaly that appears to reside in the transition zone; apparent connections to features A and E (Figure 9, B-B′ and C-C′) resemble rays and may be smearing artifacts. It is unlikely that G itself is an artifact, as it extends horizontally beneath a low-velocity zone (Figure 9, section C-C′).

[35] Figure 10 shows results from a synthetic resolution test including structures comparable to the lithospheric features (A through F) detected in the tomographic model. All features were assigned anomalies (positive or negative) of 1.5% and thicknesses of 250 km (representing the approximate maximum thickness of the lithosphere in the Superior) [*Darbyshire et al.*, 2007]; a noise level comparable to the real data was added, as in the checkerboard test. The plan-view result shows that the inversion will locate sharp lateral velocity changes with great precision and that smearing and

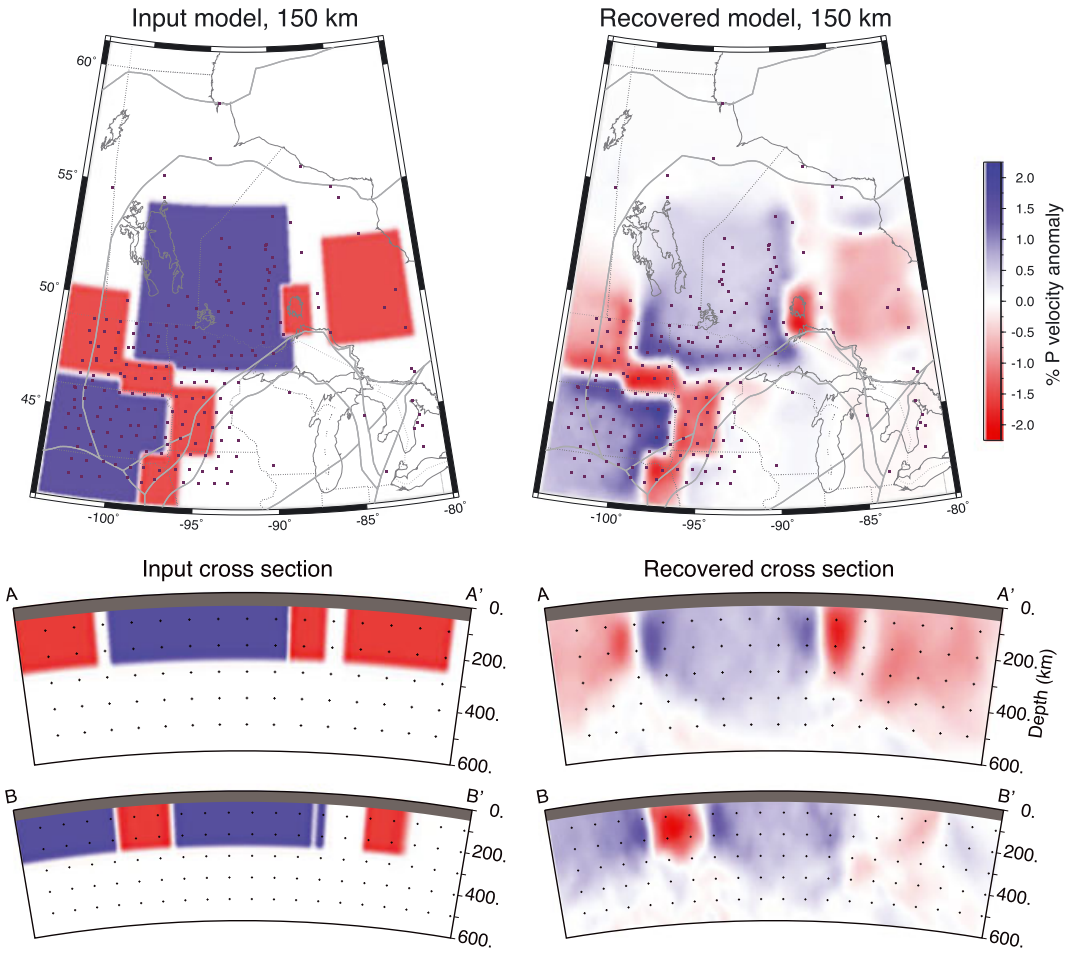

Figure 10. Structural resolution test, measuring the degree of lateral and downward smearing of lithospheric features similar to those found in the model. Cross-section locations are shown in Figure 9.

excessive smoothing are only likely in regions with very poor coverage. However, broad regions of constant lithospheric velocity appear weaker than in the input model. This is probably a consequence of the use of relative travel-times and station corrections in the inversion. A large block of constant velocity will produce an absolute traveltime residual but little relative traveltime difference between stations overlying the block. Furthermore, an instrument in the center of a laterally invariant feature will not see much directional traveltime variation due to the feature, and so its influence will be static (and so assignable to a station term). Finally, a regularized inversion with a non-zero damping component (necessary for numerical stability) will always tend to reduce anomaly amplitudes. The consequence of these factors is that the type of tomography used here is relatively insensitive to very long-wavelength structures and so sees a "band-passed" version of Earth structure.

[36] The structural test is most useful in evaluating the degree of vertical smearing likely to be present in the true model. The cross sections show that downward smearing (along near-vertical ray paths) is a major factor in the recovered model. In particular, feature A appears to reach depths of 350 km or greater in Figure 9, but the synthetic test (Figure 10, cross sections) is strong evidence that the feature is probably confined to the lithosphere. The apparent differences in thickness between the larger and smaller features is also probably an artifact (compare features A, B, and C in section A-A′), in that broader features experience a larger degree of downward smearing. The simplest interpretation is that features A through F are all confined entirely to the lithosphere, assuming a lithospheric thickness of approximately 200–250 km [as found by *Darbyshire et al.*, 2007]. Note, however, that the structural test does not generate high velocities in the location of feature G, further supporting our belief that G is not a smearing artifact.

5. Discussion

5.1. Deep High-velocity Feature: Farallon Fragment?

[37] Although the focus of this project is lithospheric, the tomographic model has significant resolution down to the base of the transition zone. The feature labeled G in Figure 8d is a sub-lithospheric high-velocity anomaly located south of 47°N, largely at and below 400 km (Figure 9). Lateral resolution in this portion of the model is generally good (Figure 7), though the depth extent of the feature is likely to be exaggerated by smearing down near-vertical ray paths.

[38] It has been known for some time [*Van der Lee and Nolet*, 1997; *Schmid et al.*, 2002] that the North American mantle contains remnants of the Farallon subduction system, preserved largely in the form of deformed slab fragments in and below the transition zone. The Farallon plate subducted

at a low angle for an extended period of time [*Liu et al*., 2008], and so slab remnants extend nearly to the eastern seaboard [*Ren et al*., 2007]. The high-velocity feature we see below 400 km is thus in a plausible position for a Farallon slab fragment. Its relatively shallow depth lies above the fragments detected by *Ren et al*. [2007] at this longitude; however, it matches a high-velocity feature detected by *Sigloch* [2011] in a comparable depth range, associated with the Laramide slab. The novel observation in our model is that our high-velocity feature G terminates at approximately 47°N; a similar termination is seen in the multi-mode *S* wave model of *Tian et al*. [2011].

[39] We have not done sufficient resolution testing to confirm that the position and shape of feature G are correct. We can therefore only raise the possibility that feature G represents a slab remnant from Farallon subduction, whose northern edge has been detected in our model. It is also important to note that feature G connects to a lithospheric high-velocity zone in section D-D′ (Figure 9), though the lithospheric high velocities are in an unresolved portion of the model volume. Future models including SPREE and further Transportable Array data will provide a wider ray aperture and so better constrain this structure's shape, position, and attitude; we will not attempt a more detailed interpretation at this time.

5.2. Western Superior Mantle Anomaly

[40] The Superior Province is associated with high velocities in global and continental-scale tomographic models [see, e.g., *Van der Lee and Frederiksen*, 2005], as well as thick (approximately 150–250 km) lithosphere [Darbyshire *et al*., 2007]. Shear-wave splits in the western Superior tend to be large [*Silver and Kaneshima*, 1993; *Kay et al*., 1999; *Frederiksen et al*., 2007], with values exceeding 2 s in some locations. The splitting measurements show a consistent WSW-ENE pattern, which is a close match to the strikes of terrane boundaries within the western Superior. The Superior lithosphere also shows internal layering at scales of ≈40 km [*Musacchio et al*., 2004; *Angus et al*., 2009] with varying anisotropic fabric, which has been attributed at least in part to terrane accretion via Archean subduction [*White et al*., 2003].

[41] We interpret the largest high-velocity region of our tomographic model (feature A) to represent this unusual western Superior mantle, due to its location, velocity, and coincidence with strong anisotropy (Figure 11). Within the western Superior lithosphere, the velocity is approximately 1.5% higher than the IASP91 base value in our model; though we note that because the tomography is not sensitive to large constant-velocity blocks (Figure 10), this is probably an underestimate. The western Superior is also a locus of strong shear-wave splitting [*Frederiksen et al*., 2007]; in Figure 11a, contours of shear-wave split times from an in-progress compilation are overlain on the tomographic model, along with arrows indicating the individual splitting measurements. There is a close correspondence between the region with split times greater than 0.8–1 s and the high-velocity western Superior feature, and fast directions in the western Superior have a consistent WSW-ENE orientation, so we interpret strong lithospheric anisotropy with this orientation to be a characteristic of the western Superior mantle anomaly.

[42] The combined high resolution and large extent of our model has enabled us to delimit the edge of the western Superior anomaly around about two thirds of its perimeter (Figure 11b), constraining its eastern, southern, and western limits. The 1 s split time contour is also helpful in delimiting this boundary. The eastern edge of the Superior anomaly was previously described by *Frederiksen et al*. [2007] as a major change in seismic velocity, anisotropy, and possibly rheology, attributed to modification of the eastern Superior lithosphere during its passage over the Great Meteor hot spot. Our new model does not change this observation of the eastern edge significantly—however, the southern and western edges are newly detected. To the southeast, the edge appears to correspond to the northwest boundary of the mid-Continent rift in the splitting contours but is not well resolved

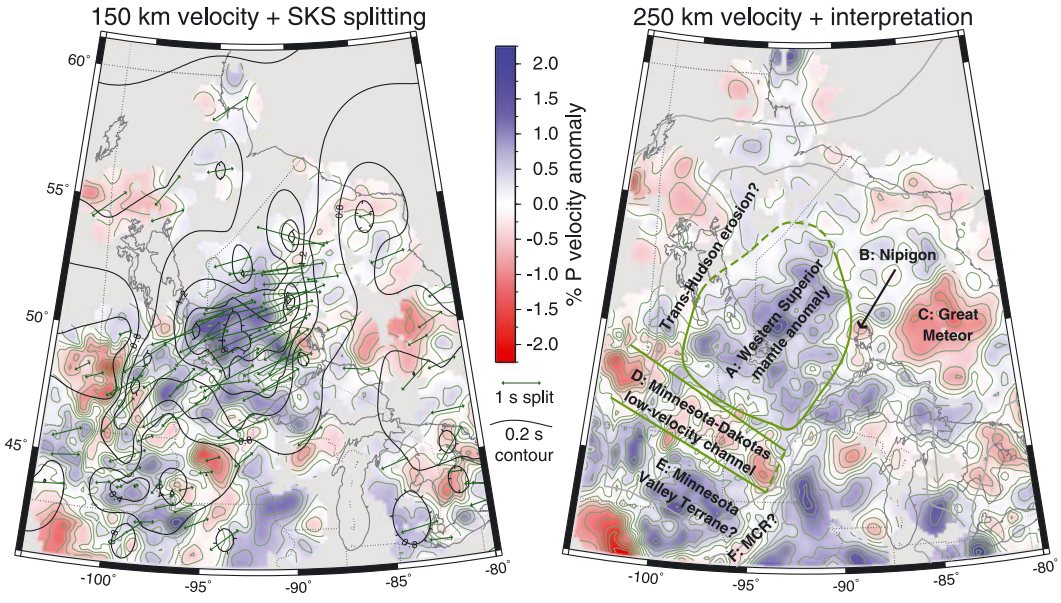

Figure 11. Left: tomography results at 150 km depth with superimposed contours of compiled shear-wave splitting times (black lines) (Frederiksen et al., in preparation) along with the individual shear-wave splitting measurements (green arrows). Right: tomography at 250 km depth with interpretation of major structures.

in the tomography. To the southwest, the velocity and splitting boundaries mark the beginning of a low-velocity channel (described below) that does not correspond to any known crustal feature; to the west, the western Superior mantle anomaly boundary is parallel to the Superior/Trans-Hudson crustal boundary, but ≈200 km east of the crustal contact.

5.3. Mid-Continent Rift

[43] At this time, we have only a limited ability to resolve the Mid-Continent Rift (MCR) itself due to the lack of instrumentation crossing the rift axis. The rift is only well covered by this data set in southern Minnesota and northwestern Iowa. In this well-covered area, we see a low-velocity anomaly (feature F) that closely corresponds to the crustal footprint of the rift (Figure 11b) and appears to be moderately well resolved (Figure 10). This is an early indication that the MCR was a lithospheric-scale feature, at least locally, and that the lithosphere beneath the rift is different to the surrounding continental material, as a result of thinning, modification, or removal of the continental lithosphere and its replacement by less-depleted mantle material.

[44] By contrast, the lithosphere beneath the Lake Superior portion of the rift appears to be high velocity in our tomographic model. However, due to the very poor station coverage in this section, and the absence of crossing rays beneath Lake Superior, it is entirely possible that what we see beneath Lake Superior is a smearing artifact from elsewhere in the model. A definitive test of the existence of a low-velocity anomaly beneath the main body of the MCR awaits further eastward movement of the EarthScope Transportable Array and the availability of data from the SPREE project [*Stein et al*., 2011; *Van der Lee et al*., 2011].

[45] Our model does, however, have good resolution of the Nipigon Embayment (feature B, Figure 11). The Nipigon Embayment is a region of basaltic magmatism surrounding Lake Nipigon, on the north shore of Lake Superior [*Hart and MacDonald*, 2007]; diabasic intrusions in the Nipigon Embayment are the oldest-known igneous rocks associated with the MCR [*Hollings et al*., 2007). Our model confirms an observation of *Frederiksen et al*. [2007] that the Nipigon Embayment overlies a low-velocity mantle anomaly. At present, due to the lack of resolution beneath Lake Superior, we are unable to determine whether the Nipigon mantle anomaly is connected to a similar anomaly beneath the main rift axis, as would be expected if the Nipigon Embayment were a failed arm of the MCR, with an origin and deep structure similar to that of the main body of the rift. If, as suggested by *Hart and MacDonald* [2007], the Nipigon Embayment is related to reactivation of pre-existing structures rather than a triple junction, then the Nipigon mantle anomaly will require another explanation, such as a pre-MCR plume track [*Hollings et al*., 2004] or the involvement of plume activity in initiating MCR rifting [*Heaman et al*., 2004].

5.4. Linear Low-Velocity Feature Beneath the Dakotas

[46] A surprising and novel feature of our tomographic model is the low-velocity channel observed beneath western Minnesota and the Dakotas, within the Superior Province (feature D; Figure 11). The feature is located in the best-resolved part of the model volume (Figure 7), and its thickness is likely to be less exaggerated by smearing than the larger features around it (Figure 10), though we cannot be certain whether it traverses the entire lithosphere. The channel trends NW-SE, crosscutting the WSW-ENE structural grain of Superior Province terrane boundaries.

[47] Our observed low-velocity channel does not correspond to any obvious crustal feature. In Minnesota, it crosscuts the Minnesota River Valley and Wawa sub-provinces, as well as the Great Lakes Tectonic Zone separating the two [*Jirsa et al*., 2011]; in North and South Dakota, the Precambrian basement is poorly exposed. There is no obvious feature in gravity (Figure 1) or magnetic anomaly maps [*Holm et al*., 2007] corresponding to the channel, suggesting that our observed mantle feature does not correspond to any major structural trend in the crust. The lack of an obvious relation to crustal features makes interpretation of the channel somewhat difficult. The southeast end of the feature does, however, appear to line up with a deflection in the Mid-Continent Rift: the Belle Plaine fault system in southeast Minnesota, which accommodates the left-lateral offset between the Superior and Iowa zones of the MCR [*Ojakangas et al*., 2001]. This correspondence is suggestive of an association between the channel and the MCR, though the nature of the association is not clear.

[48] One possible mechanism for producing a low-velocity channel is the preserved track of a mantle plume. Hot spot tracks have been known to produce linear low-velocity features in lithospheric images [see, e.g., *Rondenay et al*., 2000], and it has been suggested that a mantle plume was involved in the initiation of MCR rifting [*Heaman et al*., 2004]. No plume track has been recognized along the channel, but given the very limited Precambrian exposure in the Dakotas, it is conceivable that such a track has been missed; in Minnesota, the channel is parallel to the overall trend of mafic dikes [*Jirsa et al*., 2011], though intrusions in the area are generally coeval with the Penokean orogen rather than the MCR. It is also possible that the plume never reached the surface to any significant degree, leading to a similar situation to that described by [*Bank et al*., 1998], in which a low-velocity feature observed beneath the Trans-Hudson Orogen is attributed to a lithospheric plume track that did not break the surface.

[49] Another possibility is that the low-velocity channel is related to a failed branch of MCR rifting. The coincidence of the northeast end of the channel with the deflection of the MCR along the Belle Plaine fault system is compatible with a triple junction, and the low-velocity feature observed in the Nipigon Embayment is precedent for low velocities to coincide with MCR-related rifting. Rifting may in some cases thin the lithosphere before the crust [*Huismans and Beaumont*, 2011], and it is possible that if the rifting failed at an early stage, the effect on the crust may have been minor.

[50] The final possibility is that the low-velocity channel is an older feature preserved from Superior accretion. The Minnesota River Valley terrane (MRV), at the southwest tip of the Superior Province, is unusual in a number of ways. It is Paleoarchean in age [*Bickford et al*., 2006], though it accreted onto assembled younger terranes in the 2.68 Ga Minnesotan orogeny, the last stage of Superior cratonization [*Percival et al*., 2006]. Notably, the MRV predates the proposed ca. 3 Ga initiation of plate tectonics [*Shirey and Richardson*, 2011], and so subduction is unlikely to have played a role in the formation of the MRV lithosphere.

It is thus conceivable that the low-velocity channel preserves a zone along the boundary between domains of differently derived lithosphere, between the western Superior core and the MRV. It is worth noting, however, that though the position of the channel is fairly close to the Great Lakes Tectonic Zone (GLTZ; the crustal boundary at the northern edge of the MRV), its northwest strike is significantly different from the interpreted southwest strike of the GLTZ. Thus, in order for the channel to be a preserved accretionary feature, the mantle boundary would need to be displaced and skewed relative to its crustal equivalent.

[51] At the moment, we are unable to make a definitive interpretation of the low-velocity channel. Further SPREE and Transportable Array data will expand model resolution across the MCR and so clarify the relationship between the channel and other tectonic elements. It may also be possible to examine crustal thickness across the channel using receiver function analysis and so determine whether any crustal thinning has taken place along the channel. If such thinning were to be detected, it would be strong evidence in favor of the rift-branch hypothesis.

5.5. Modification History of the Superior Lithospheric Root

[52] Assuming our basic interpretation of the observed features is correct, the novel features observed in this study may be tentatively associated with specific events in the history of central North America and so placed upon an approximate timeline. The oldest features in our model are presumably those associated with Archean Superior crust (features A and E, Figure 11). The Western Superior mantle anomaly (feature A) is likely of Archean accretionary origin, which has led to a strong anisotropic fabric parallel to the strike of accreted terranes [see, e.g., *Frederiksen et al*., 2007]. By contrast, the Minnesota River Valley terrane, which shows less evidence of Archean plate tectonics, displays weak to nonexistent anisotropy and may have developed through mechanisms other than subduction.

[53] The next major event in the history of the study area was the ca. 1.8 Ga Trans-Hudson Orogen, which for the most part lies west of our study area. Our results indicate that the lithospheric contact between the Superior Province and Trans-Hudson lies approximately 200 km east of the crustal contact, i.e., that the Western Superior anomaly ends significantly inboard of the crustal limits of the Superior. Given that the Superior/Trans-Hudson contact crosscuts the Superior's internal tectonic subdivisions, it is likely that the Superior mantle root originally extended further west and was eroded or modified by processes associated with Trans-Hudson orogenesis. Nearly contemporaneously with the Trans-Hudson, the Penokean Orogen took place southeast of the Western Superior anomaly, but its influence has been overprinted by the Mid-Continent Rift and is difficult to recognize in our model.

[54] The ca. 1.1 Ga Mid-Continent Rift is only imaged by this model in a relatively small area, but shows indications of a low-velocity channel (feature F) which may represent rifting of the cratonic root and emplacement of more fertile mantle material, and is tentative evidence that the MCR affected the full thickness of the continental lithosphere as well as the crust. The Nipigon Embayment feature (B), regardless of the specifics of its origin, is likely to be MCR related and roughly contemporaneous; if the failed-rift-arm hypothesis for the Dakotas low-velocity channel is correct, its age is also approximately the same. The close alignment of the observed features with surface tectonics indicates that the lithosphere in the study area has not been significantly deformed for at least 1 Ga.

[55] The youngest feature visible in the model is a small section of the Great Meteor hot spot track (feature C), which is a well-known feature of the eastern North American lithosphere [see, e.g., *Rondenay et al*., 2000]. The presence of this feature is evidence that hot spot tracks can make long-lived changes to the continental lithosphere. A possible offset between the mantle image of the Great Meteor track and its crustal expression [*Eaton and Frederiksen*, 2007] indicates that parts of the continental mantle may be deformable and so that the Western Superior anomaly may have a different rheology from the zone of Great Meteor influence [*Frederiksen et al*., 2007].

6. Conclusion

[56] The mantle image presented in this study represents a high-resolution image of structures preserving evidence of 3 Ga of lithospheric processes. We have delineated a region of anomalous high-velocity, strongly anisotropic mantle beneath the western Superior province that may represent an accretionary nucleus of Archean lithosphere and found that the boundaries of this region are different from those of the crustal Superior Province. In particular, its western edge lies approximately 200 km east of the crustal Superior/Trans-Hudson contact, suggesting erosion ca. 1.8 Ga. To the southwest, the western Superior anomaly is truncated by a low-velocity channel of uncertain origin, which may possibly be related to the ca. 1.1 Ga Mid-Continent Rift, beyond which high velocities resume beneath the Minnesota River Valley terrane. The Mid-Continent Rift itself is only beginning to be resolved; its relationship to the features described here will be further elucidated with the arrival of further data from project SPREE.

[57] **Acknowledgments.** Manitoba instruments were deployed with the logistical assistance of Manitoba Hydro, the Geological Survey of Canada, Agriculture Canada, and Vale Limited, with field assistance from Mulu Serzu, John McCutcheon, Troy Unrau, and Oluwaseyi Idowu. Manitoba instruments were funded by a grant from the Canadian Foundation for Innovation. Data from CNSN and POLARIS instruments were obtained from the Geological Survey of Canada online data archive; EarthScope data were obtained from the IRIS Data Management Center. Mapping was performed using the GMT software package. This research was funded by an NSERC grant.

References

Angus, D., J. Kendall, D. Wilson, D. J. White, S. Sol, and C. J. Thomson (2009), Stratigraphy of the Archean western Superior Province from P-and S-wave receiver functions: Further evidence for tectonic accretion? *Phys. Earth Planet Int.*, *117*, 206–216, doi:10.1016/j.pepi.2009.09.002.

Ansdell, K. (2005), Tectonic evolution of the Manitoba-Saskatchewan segment of the Paleoproterozoic Trans-Hudson Orogen, Canada, *Can. J. Earth Sci.*, *42*, 741–759, doi:10.1139/E05-035.

Bank, C., M. Bostock, R. Ellis, Z. Hajnal, and J. VanDecar (1998), Lithospheric mantle structure beneath the Trans-Hudson Orogen and the origin of diamondiferous kimberlites, *J. Geophys. Res.*, *103*, 10,103–10,114.

Bassin, C., G. Laske, and G. Masters (2000), The current limits of resolution for surface wave tomography in North America, *EOS Trans AGU*, *81*, F897.

Bickford, M. E., J. L. Wooden, and R. L. Bauer (2006), SHRIMP study of zircons from Early Archean rocks in the Minnesota River Valley: Implications for the tectonic history of the Superior Province, *Geol. Soc. Am. Bull.*, *118*, 94–108, doi:10.1130/B25741.1.

Calvert, A. J., and J. N. Ludden (1999), Archean continental assembly in the southeastern Superior Province of Canada, *Tectonics*, *18*, 412–429.

Calvert, A. J., E. W. Sawyer, W. J. Davis, and J. N. Ludden (1995), Archean subduction inferred from seismic images of a mantle suture in the Superior Province, *Nature*, *375*, 670–674.

Cannon, W. F. (1994), Closing of the Midcontinent Rift—a far-field effect of Grenvillian compression, *Geology*, *22*, 155–158.

Card, K. D., and K. H. Poulsen (1998), Geology and mineral deposits of the Superior Province of the Canadian Shield, in *Geology of the Precambrian Superior and Grenville Provinces and Precambrian Fossils in North America, Geology of North America*, vol. C-1, edited by S. B. Lucas, and M. R. St-Onge, pp. 13–204, Geological Survey of Canada, Ottawa.

Darbyshire, F. A. and D. W. Eaton (2010), The lithospheric root beneath Hudson Bay, Canada from Rayleigh wave dispersion: no clear seismological distinction between Archean and Proterozoic mantle, *Lithos*, *120*, 144–159, doi:10.1016/j.lithos.2010.04.010.

Darbyshire, F. A., D. W. Eaton, A. W. Frederiksen, and L. Ertolahti (2007), New insights into the lithosphere beneath the Superior Province from Rayleigh wave dispersion and receiver function analysis, *Geophys. J. Int.*, *169*, 1043–1068, doi:10.1111/j.1365-246X.2006.03259.x.

Eaton, D. W., and A. W. Frederiksen (2007), Seismic evidence for convection-driven motion of the North American plate, *Nature*, *446*, 428–431, doi:10.1038/nature05675.

Eaton, D., A. Frederiksen, and S.-K. Miong (2004), Shear-wave splitting observations in the lower Great Lakes region: Evidence for regional anisotropic domains and keel-modified asthenospheric flow, *Geophys. Res. Lett.*, *31*, doi:10.1029/2004GL019438.

Ferguson, I. J., J. A. Craven, R. D. Kurtz, D. E. Boerner, R. C. Bailey, X. Wu, M. R. Orellana, J. Spratt, G. Wennberg, and M. Norton (2005), Geoelectric response of Archean lithosphere in the western Superior Province, central Canada, *Phys. Earth Planet. Int.*, *150*, 123–143, doi:10.1016/j.pepi.2004.08.025.

Foley, S. F. (2008), Rejuvenation and erosion of the cratonic lithosphere, *Nat. Geosci.*, *1*, 503–509, doi:10.1038/ngeo261.

Frederiksen, A. W., S.-K. Miong, F. A. Darbyshire, D. W. Eaton, S. Rondenay, and S. Sol (2007), Lithospheric variations across the Superior Province, Ontario, Canada: Evidence from tomography and shear wave splitting, *J. Geophys. Res.*, *112*, B07318, doi:10.1029/2006JB004861.

Hart, T. R., and C. A. MacDonald (2007), Proterozoic and Archean geology of the Nipigon Embayment: Implications for emplacement of the Mesoproterozoic Nipigon diabase sills and mafic to ultramafic intrusions, *Can. J. Earth Sci.*, *44*, 1021–1040, doi:10.1139/EO7-026.

Heaman, L., B. Kjarsgaard, and R. Creaser (2004), The temporal evolution of north American kimberlites, *Lithos*, *76*, 377–397, doi:10.1016/j.lithos.2004.03.047.

Hoffman, P. F. (1988), United plates of America, the birth of a craton: Early Proterozoic assembly and growth of Laurentia, *Ann. Rev. Earth Planet. Sci.*, *16*, 543–603.

Hoffman, P. F. (1989), Precambrian geology and tectonic history of North America, in *The Geology of North America—An Overview*, edited by A. W. Bally, and A. R. Palmer, pp. 447–512, Geological Society of America, Boulder, CO.

Hollings, P., P. Fralick, and S. Kissin (2004), Geochemistry and geodynamic implications of the Mesoproterozoic English Bay graniterhyolite complex, northwestern Ontario, *Can. J. Earth Sci.*, *41*, 1329–1338, doi:10.1139/e04-077.

Hollings, P., P. Fralick, and B. Cousens (2007), Early history of the Midcontinent Rift inferred from geochemistry and sedimentology of the Mesoproterozoic Osler Group, northwestern Ontario, *Can. J. Earth Sci.*, *44*, 389–412, doi:10.1139/E06-084.

Holm, D. K., R. Anderson, T. J. Boerboom, W. F. Cannon, V. Chandler, M. Jirsa, J. Miller, D. Schneider, K. J. Schulz, and W. R. Van Schmus (2007), Reinterpretation of Paleoproterozoic accretionary boundaries of the north-central United States based on anew aeromagnetic-geologic compilation, *Precambrian Res.*, *157*, 71–79, doi:10.1016/j.precamres.2007.02.023.

Huismans, R., and C. Beaumont (2011), Depth-dependent extension, two-stage breakup and cratonic underplating at rifted margins, *Nature*, *473*, 74–78, doi:10.1038/nature09988.

Jirsa, M. A., T. J. Boerboom, V. W. Chandler, J. H. Mossler, A. C. Runkel, and D. R. Setterholm (2011), Geologic map of Minnesota—bedrock geology, in *Minnesota Geological Survey State Map Series S-21*, scale 1:500,000, Minnesota Geological Survey, St. Paul.

Jordan, T. H. (1978), Composition and development of the continental tectosphere, *Nature*, *274*, 544–548.

Kay, I., S. Sol, J. Kendall, C. Thomson, D. J. White, I. Asudeh, B. Roberts, and D. Francis (1999), Shear wave splitting observations in the Archean craton of Western Superior, *Geophys. Res. Lett.*, *26*, 2669–2672.

Kennett, B. L. N. and E. R. Engdahl (1991), Traveltimes for global earthquake location and phase identification, *Geophys. J. Int.*, *105*, 429–465.

Liu, Q. and Y. J. Gu (2012), Seismic imaging: From classical to adjoint tomography, *Tectonophysics*, *566–567*, 31–66, doi:10.1016/j.tecto.2012.07.006.

Li, C., R. D. van der Hilst, E. R. Engdahl, and S. Burdick (2008), A new global model for P wave speed variations in Earth's mantle, *Geochem. Geophys. Geosyst.*, *9*, Q05018, doi:10.1029/2007GC001806.

Liu, L., S. Spasojevic, and M. Gurnis (2008), Reconstructing Farallon plate subduction beneath North America back to the Late Cretaceous, *Science*, *322*, 934–938, doi:10.1126/science.1162921.

Mariano, J., and W. Hinze (1994), Structural interpretation of the Midcontinent Rift in eastern Lake Superior from seismic reflection and potential-field studies, *Can. J. Earth Sci.*, *31*, 619–628.

Musacchio, G., D. J. White, I. Asudeh and C. J. Thomson (2004), Lithospheric structure and composition of the Archean western Superior Province from seismic refraction/wide-angle reflection and gravity modelling, *J. Geophys. Res.*, *109*, B03304, doi:10.1029/2003JB002427.

Németh, B., R. M. Clowes, and Z. Hajnal (2005), Lithospheric structure of the Trans-Hudson Orogen from seismic refraction-wide-angle reflection studies, *Can J. Earth Sci.*, *42*(4), 435–456, doi:10.1139/e05-032.

Nicholson, S., S. Shirey, K. Schulz, and J. Green (1997), Rift-wide correlation of 1.1 Ga midcontinent rift system basalts: Implications for multiple mantle sources during rift development, *Can. J. Earth Sci.*, *34*, 504–520.

North, R. G., and P. W. Basham (1993), Modernization of the Canadian National Seismograph Network, *Seis. Res. Let.*, *64*, 41.

Ojakangas, R., G. Morey, and J. Green (2001), The Mesoproterozoic Midcontinent Rift System, Lake Superior Region, USA, *Sediment. Geol.*, *141*, 421–442.

Osmani, I. A. (1991), Proterozoic mafic dyke swarms in the Superior Province of Ontario, in *Geology of Ontario*, *Ontario Geological Survey Special Volume 4, Part 1*, edited by P. C. Thurston, H. R. Williams, R. H. Sutcliffe, and G. M. Stott, pp. 661–681, Ontario Geological Survey, Toronto.

Parker, R. L. (1994), *Geophysical Inverse Theory*, 366 pp., Princeton University Press, Princeton, NJ.

Pearson, D. G. and N. Wittig (2008), Formation of Archaean continental lithosphere and its diamonds: The root of the problem, *J. Geol. Soc. London*, *165*, 895–914, doi:10.1144/0016-76492008-003.

Percival, J. A. and G. F. West (1994), The Kapuskasing uplift: A geological and geophysical synthesis, *Can. J. Earth Sci.*, *31*, 1256–1286.

Percival, J. A., M. Sanborn-Barrie, T. Skulski, G. M. Stott, H. Helmstaedt, and D. J. White (2006), Tectonic evolution of the western Superior Province from NATMAP and Lithoprobe studies, *Can. J. Earth Sci.*, *43*, 1085–1117, doi:10.1139/e06-062.

Ren, Y., E. Stutzmann, R. van der Hilst, and J. Besse (2007), Understanding seismic heterogeneities in the lower mantle beneath the Americas from seismic tomography and plate tectonic history, *J. Geophys. Res.*, *112*, B01302, doi:10.1029/2005JB004154.

Rondenay, S., M. G. Bostock, T. M. Hearn, D. J. White and R. M. Ellis (2000), Lithospheric assembly and modification of the SE Canadian Shield: Abitibi-Grenville teleseismic experiment, *J. Geophys. Res.*, *105*, 13,735–13,754.

Schmid, C., S. Goes, S. van der Lee, and D. Giardini (2002), Fate of the Cenozoic Farallon slab from a comparison of kinematic thermal modeling with tomographic images, *Earth Plan. Sci. Lett.*, *204*, 17–32, doi:10.1016/S0012-821X(02)00985-8.

Schulz, K., and W. F. Cannon (2007), The Penokean orogeny in the Lake Superior region, *Precambrian Res.*, *157*, 4–25, doi:10.1016/j.precamres.2007.02.022.

Sexton, J., and H. Henson Jr (1994), Interpretation of seismic reflection and gravity profile data in western Lake Superior, *Can. J. Earth Sci.*, *31*, 652–660.

Shirey, S. B., and S. H. Richardson (2011), Start of the Wilson Cycle at 3 Ga shown by diamonds from subcontinental mantle, *Science*, *333* (6041), 434436, doi:10.1126/science.1206275.

Sigloch, K. (2011), Mantle provinces under North America from multifrequency *P* wave tomography, *Geochem. Geophys. Geosyst.*, *12*, Q02W08, doi:10.1029/2010GC003421.

Silver, P., and S. Kaneshima (1993), Constraints on mantle anisotropy beneath Precambrian North America from a transportable teleseismic experiment, *Geophys. Res. Lett.*, *20*, 1127–1130.

Silver, P. G., R. P. Meyer and D. E. James (1993), Intermediate-scale observations of the Earth's deep interior from the APT89 transportable teleseismic experiment, *Geophys. Res. Lett.*, *20*, 1123–1126.

Sol, S., C. J. Thomson, J.-M. Kendall, D. White, J. C. VanDecar and I. Asudeh (2002), Seismic tomographic images of the cratonic upper mantle beneath the Western Superior Province of the Canadian Shield—A remnant Archean slab? *Phys. Earth Planet. Inter.*, *134*, 53–69, doi:10.1016/S0031-9201(02)00081-X.

Stein, S., et al. (2011), Learning from failure: The SPREE Mid-Continent Rift experiment, *GSA Today*, *21*, 5–7, doi:10.1130/G120A.1.

Tanner, J. G., et al. (1988), Gravity anomaly map of North America, *The Leading Edge*, *7*, 15–18.

Tian, Y., Y. Zhou, K. Sigloch, G. Nolet, and G. Laske (2011), Structure of North American mantle constrained by simultaneous inversion of

multiple-frequency SH, SS, and Love waves, *J. Geophys. Res.*, *116*, B02307, doi:10.1029/2010JB007704.

VanDecar, J. (1991), Upper-mantle structure of the Cascadia subduction zone from non-linear teleseismic travel-time inversion, Ph.D. thesis, University of Washington, Seattle, 165 pp.

VanDecar, J. C. and R. S. Crosson (1991), Determination of teleseismic relative phase arrival times using multi-channel cross correlation and least squares, *Bull. Seis. Soc. Am.*, *80*, 150–169.

Van der Lee, S. and SPREE team (2011), SPREE: Field experiment to study deep structure of the mid-continent rift, *Geol. Soc. Am. Abstr. Programs*, *43*(5), 549.

Van der Lee, S., and A. Frederiksen (2005), Surface wave tomography applied to the North American upper mantle, in *Seismic Earth: Array Analysis of Broadband Seismograms, Geophysical Monograph Series*, vol. 157, edited by A. Levander, and G. Nolet, pp. 67–80, AGU, Washington D. C., doi:10.1029/157GM05.

van der Lee, S., and G. Nolet (1997), Seismic image of the subducted trailing fragments of the Farallon plate, *Nature*, *386*, 266–269.

Van Schmus, W., and W. Hinze (1985), The midcontinent rift system, *Ann. Rev. Earth Planet. Sci.*, *13*, 345–383.

White, R. (1997), Mantle temperature and lithospheric thinning beneath the Midcontinent rift system: Evidence from magmatism and subsidence, *Can. J. Earth Sci.*, *34*, 464–475.

White, D. J., G. Musacchio, H. H. Helmstaedt, R. M. Harrap, P. C. Thurston, A. Van der Velden and K. Hall (2003), Images of a lower-crustal oceanic slab: Direct evidence for tectonic accretion in the Archean western Superior province, *Geology*, *31*, 997–1000, doi:10.1130/G20014.1.

Whitmeyer, S. J. and K. E. Karlstrom (2007), Tectonic model for the Proterozoic growth of North America, *Geosphere*, *3*, 220–259, doi: 10.1130/GES00055.1.

Williams, M. L., K. M. Fischer, J. T. Freymueller, B. Tikoff, A. M. Tréhu, and others (2010), Unlocking the Secrets of the North American Continent: An EarthScope Science Plan for 2010–2020, 78 pp.

Zhang, H.-F., M. Sun, X.-H. Zhou, M.-F. Zhou, W.-M. Fan, and J. P. Zheng (2003), Secular evolution of the lithosphere beneath the eastern North China Craton: Evidence from Mesozoic basalts and high-Mg andesites, *Geochim. Cosmochim. Acta*, *67*, 4373–4387, doi:10.1016/S0016-7037(03)00377-6.

Zhu, R. X. and T. Y. Zheng (2009), Destruction geodynamics of the North China Craton and its Paleoproterozoic plate tectonics, *Chinese Sci Bull*, *54*, 3354–3366, doi:10.1007/s11434-009-0451-5.